Physical Layer Security in Near-Field Communications

Zheng Zhang, Yuanwei Liu, Zhaolin Wang, Xidong Mu, and Jian Chen

***Abstract*—A near-field secure transmission framework is proposed. Employing the hybrid beamforming architecture, a multi-antenna base station (BS) transmits confidential information to a multi-antenna legitimate user (U) against a multi-antenna internal eavesdropper (E) in the near field. Based on the spherical-wave channel state information of U and E, a two-stage algorithm is proposed to maximize the near-field secrecy capacity. In the first stage, the fully-digital beamformers are optimized. Then, the optimal analog beamformers and baseband digital beamformers are alternatingly derived in the closed-form expressions in the second stage. Numerical results demonstrate that in contrast to the far-field secure communication relying on the *angular disparity*, the near-field secure communication mainly relies on the *distance disparity* between U and E.**

***Index Terms*—Beam focusing, near-field communications, physical layer security.**

I. Introduction

To fulfill the growing demands for the ubiquitous connectivity of the sixth generation (6G) wireless communications, tremendous efforts have been devoted to devising emerging technologies, e.g., millimeter wave (mmWave), terahertz (THz), and ultra-massive multiple-input-multiple-output (UM-MIMO) [1]. However, all these key enablers rely on the employment of large-scale antennas and high frequencies, which inevitably causes wireless communications to be operated in the near-field region. In contrast to the conventional *planar-wave* channel model of far-field scenarios, electromagnetic (EM) propagation is accurately characterized by the *spherical-wave* channel model [2] in near-field communications. The unique spherical-wave propagation model contains both the direction and distance information of the receiver, which makes array radiation patterns focus on a specific point (i.e., *beam focusing*) of the free space. Thus, near-field communications can utilize the new dimension of distance to achieve more precise signal enhancement, which brings new opportunities to wireless communications, such as accurate interference management [2], enhanced multiplexing gains [3], and simultaneous angle and distance estimation [4], and has drawn a wide range of attention recently [5], [6].

Due to the broadcast characteristics of wireless channels, the transmitted signal is exposed to vulnerable environments and is easily wiretapped by the malicious eavesdropper (E). As a complement to cryptography, physical layer security (PLS) is proposed to safeguard private information from eavesdropping. PLS is capable of exploiting the physical characteristics of wireless channels, e.g., interference, fading, noise, directivity, and disparity, without introducing complicated secret key generation and management. Nevertheless, most works for PLS mainly focused on the planar-wave channel model of the far field [7]–[10], which may be inaccurate in characterizing the wireless signal propagation under the large-scale array antenna setup and restricts the security gains that arise from spatial beamforming. As shown in the left side of Fig. 1, the conventional secrecy *beam steering* schemes generally utilize the angular dimension to provide security in far-field communications. However, the E tends to be located in security-blind zones to wiretap the legitimate user (U) in practice, e.g., the positions between the base station (BS) and the U as depicted in the right side of Fig. 1, because in this case the BS cannot effectively suppress or interfere with the eavesdropper. To guarantee a positive gap between the channel capacities of the legitimate user and the eavesdropper, there has been a preliminary study that considers an extremely large-scale array at the BS and exploits the distance dimension contained in the spherical-wave channel to secure wireless communications [11]. However, the dedicated secrecy beam focusing strategy for near fields still lacks investigation as the near-field channel model brings a new challenge to the secrecy beamforming design of MIMO networks. To elaborate, near-field transmission requires a larger hybrid beamforming structure than that of far-field networks due to the fact that it brings more degrees of freedom (DoFs) for parallel stream transmission. Therefore, computationally efficient secrecy hybrid beamforming optimization algorithms are demanded to secure near-field transmission[1]. Therefore, it becomes essential to develop the secrecy beam focusing scheme for near fields, which motivates this work.

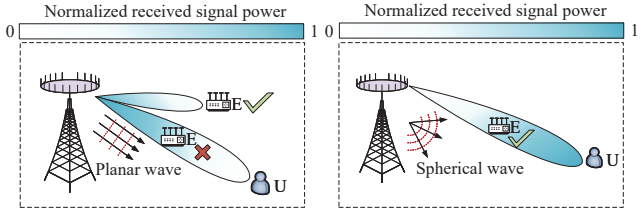

Fig. 1. Comparison of secure transmission in far-field and near-field networks. Left side: far-field secure communication using beam steering; right side: near-field secure communication using beam focusing.

To exploit the security gains offered by near-field channels, this paper proposes a near-field secure transmission framework, where the beam focusing is exploited at the BS to convey confidential information to a legitimate user in the presence of an eavesdropper located between the legitimate user and the BS. The hybrid beamforming architecture is

Zheng Zhang and Jian Chen are with the School of Telecommunications Engineering, Xidian University, Xi'an 710071, China (e-mail: zzhang_688@stu.xidian.edu.cn; jianchen@mail.xidian.edu.cn).

Yuanwei Liu is with the School of Electronic Engineering and Computer Science, Queen Mary University of London, E1 4NS London, U.K., and also with the Department of Electronic Engineering, Kyung Hee University, Yongin-si, Gyeonggi-do 17104, South Korea (e-mail: yuanwei.liu@qmul.ac.uk).

Zhaolin Wang and Xidong Mu are with the School of Electronic Engineering and Computer Science, Queen Mary University of London, London E1 4NS, U.K. (e-mail: zhaolin.wang@qmul.ac.uk; xidong.mu@qmul.ac.uk;).

[1]Near-field study also poses a challenge to PLS analysis. In particular, the wireless channels tend towards deterministic from random in near fields. It indicates that the conventional secrecy analysis framework devoted to the fading-channel scenarios may not be applicable, which requires a new analysis technique for secrecy performance evaluation, such as the effective degrees of freedom (EDoF) approximation method [12]. However, this is out of the scope of this paper, which will direct our future work.

employed at the BS to reduce the radio frequency (RF) chain overhead. A secrecy capacity maximization problem is formulated subject to the analog phase-shift constraints and the baseband digital transmit power budget. A two-stage algorithm is developed to efficiently solve the resulting non-convex problem. Based on the fully-digital beamformers optimized in the first stage, the optimal analog precoders and baseband digital beamformers are alternatingly derived in closed-form expressions. Numerical results demonstrate the convergence of the proposed two-stage algorithm. It also reveals that: 1) the proposed hybrid beamforming scheme can achieve comparable performance to the fully-digital strategy; and 2) the secrecy performance in the near-field systems relies on the distance from the E to the reference point of the U, irrespective of the angle with respect to the BS.

II. System Model and Problem Formulation

A. System Model

We consider a near-field MIMO communication system, which consists of a BS, a U, and a potential E[2]. The uniform linear array (ULA) is adopted for all the nodes, where the BS is equipped with an extremely large-scale array of $M \gg 1$ antennas while the U and the E are equipped with a normal-scale array of $M \gg M_{\mathrm{U}} > 1$ and $M \gg M_{\mathrm{E}} > 1$ antennas. The antenna aperture at the BS is assumed to be D. The BS operates in the high-frequency band (e.g., mmWave or THz), and tries to send the confidential signal to the U in the presence of the E. Both U and E are located in the near-field region. The distance between the BS and U/E is assumed to be shorter than Rayleigh distance $d_{\mathrm{R}} = \frac{2(D_1+D_2)^2}{\lambda}$ (λ is the wavelength, D_1 is the antenna aperture of the BS and D_2 is the antenna aperture of U). Thus, the transmitted wavefronts follow the spherical propagation. We consider a challenging secure communication scenario, where the E is located in the same direction as the U but closer to the BS than the U. To resist the wiretapping of the E, the BS exploits the beam focusing to enhance the received signal strength at the U while suppressing the information leakage to the E. Here, we assume that the E is an internal eavesdropping node, which is served by the BS but is not trusted by the U from the perspective of data. Consequently, the perfect channel state information (CSI) of legitimate and eavesdropping channels can be obtained via the orthogonal matching pursuit method (OMP) [13].

In near-field systems with a large number of antennas, the fully-digital beamforming architecture imposes high hardware costs as it requires each antenna to be equipped with a dedicated RF chain. As a result, the hybrid beamforming architecture at the BS is considered [14]. To elaborate, a phase-shift-based analog precoder is installed between M_{R} ($M_{\mathrm{R}} < M$) RF chains and the transmit antenna array, where each output of RF chain is sent to all the transmit antennas

[2]A typical example of the considered system is the outdoor-to-indoor (O2I) network. For instance, a BS with ultra-large array antennas is located on the rooftop of the building and simultaneously serves the near user inside the building (which could be a mobile user located within ten meters) and the far user outside the building (which could be the vehicle node located within a hundred meters). However, the indoor user may be a potentially malicious eavesdropper that is interested in the information of the vehicle user.

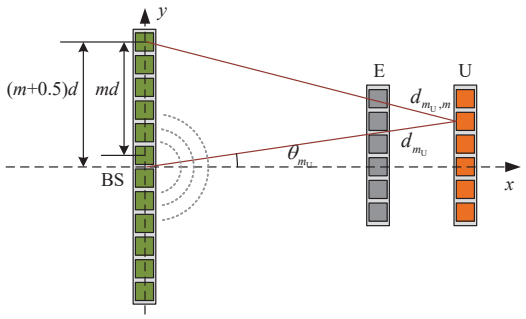

Fig. 2. The top view of the near-field MIMO network.

to form the directional spatial beamformers. Then, K data streams are transmitted to the M transmit antennas via M_{R} RF chains, which are subject to $K \le M_{\mathrm{R}} \le M$. As a result, the transmitted signal at the BS can be expressed as

$$\mathbf{s} = \mathbf{P}\mathbf{W}\mathbf{x}, \tag{1}$$

where $\mathbf{P} \in \mathbb{C}^{M \times M_{\mathrm{R}}}$ denotes the analog precoding matrix, $\mathbf{W} \in \mathbb{C}^{M_{\mathrm{R}} \times K}$ denotes the digital baseband beamforming matrix, and $\mathbf{x} \in \mathbb{C}^{K \times 1}$ ($\mathbb{E}(\mathbf{x}\mathbf{x}^H) = \mathbf{I}_K$) denotes the data intended for U. Note that the i-th row and the j-th column element of $\mathbf{P}$ satisfies

$$p_{i,j} \in \mathcal{P} \triangleq \left\{ e^{\jmath\vartheta} | \vartheta \in (0, 2\pi] \right\}, \tag{2}$$

where ϑ represents the phase shift manipulation of $p_{i,j}$. With this process, the received signals at U and E are given by

$$\mathbf{y}_{\mathrm{U}} = \mathbf{H}_{\mathrm{B,U}}\mathbf{s} + \mathbf{n}_{\mathrm{U}}, \tag{3}$$

$$\mathbf{y}_{\mathrm{E}} = \mathbf{H}_{\mathrm{B,E}}\mathbf{s} + \mathbf{n}_{\mathrm{E}}, \tag{4}$$

where $\mathbf{H}_{\mathrm{B,U}} \in \mathbb{C}^{M_{\mathrm{U}} \times M}$ and $\mathbf{H}_{\mathrm{B,E}} \in \mathbb{C}^{M_{\mathrm{E}} \times M}$ denote the equivalent channels from the BS to U and E, $\mathbf{n}_{\mathrm{U}} \sim \mathcal{CN}(0, \sigma^2\mathbf{I}_{M_{\mathrm{U}}})$ and $\mathbf{n}_{\mathrm{E}} \sim \mathcal{CN}(0, \sigma^2\mathbf{I}_{M_{\mathrm{E}}})$ denote the additive white Gaussian noise (AWGN) at the U and E, respectively. Accordingly, the mutual information between the BS and U/E is given by

$$C_{\mathrm{U}} = \log_2 \det\left(\mathbf{I}_{M_{\mathrm{U}}} + \sigma^{-2}\mathbf{H}_{\mathrm{B,U}}\mathbf{P}\mathbf{W}\mathbf{W}^H\mathbf{P}^H\mathbf{H}_{\mathrm{B,U}}^H\right), \tag{5}$$

$$C_{\mathrm{E}} = \log_2 \det\left(\mathbf{I}_{M_{\mathrm{E}}} + \sigma^{-2}\mathbf{H}_{\mathrm{B,E}}\mathbf{P}\mathbf{W}\mathbf{W}^H\mathbf{P}^H\mathbf{H}_{\mathrm{B,E}}^H\right). \tag{6}$$

Following the information-theoretic PLS, the secrecy performance can be characterized by the secrecy capacity, which is defined as the positive difference between the legitimate mutual information and the eavesdropping mutual information, i.e., $C_{\mathrm{s}} = [C_{\mathrm{U}} - C_{\mathrm{E}}]^+$, where $[x]^+ = \max\{x, 0\}$ [9].

B. Near-Field Channel Model

As shown in Fig. 2 we assume that the coordinate of the midpoint of the BS antenna is $(0, 0, 0)$. Thus, the m-th antenna of the BS can be denoted as $(0, \tilde{m}d, 0)$, where $\tilde{m} = m - \frac{M-1}{2}$ and d denotes the antenna pitch. Similarly, the coordinates of the m_{U}-th antenna at the U and the m_{E}-th antenna at the E can be denoted as $(x_{\mathrm{U}}, y_{\mathrm{U}} + \tilde{m}_{\mathrm{U}}d, 0)$ and $(x_{\mathrm{E}}, y_{\mathrm{E}} + \tilde{m}_{\mathrm{E}}d, 0)$, where $\tilde{m}_{\mathrm{U}} = m_{\mathrm{U}} - \frac{M_{\mathrm{U}}-1}{2}$ and $\tilde{m}_{\mathrm{E}} = m_{\mathrm{E}} - \frac{M_{\mathrm{E}}-1}{2}$. Accordingly, the line-of-sight (LoS) near-field channel between the BS and U can be modeled as

$$\mathbf{H}_{\mathrm{B,U}}(d, \theta) = \left[\mathbf{h}_{\mathrm{B,U},1}, \cdots, \mathbf{h}_{\mathrm{B,U},M_{\mathrm{U}}}\right]^T, \tag{7}$$

where $\mathbf{h}_{\mathrm{B,U},m_{\mathrm{U}}} = \left(1/\sqrt{M}\right)\left[g_{m_{\mathrm{U}},1}e^{-\jmath\frac{2\pi f}{c}(d_{m_{\mathrm{U}},1} - d_{m_{\mathrm{U}}})}, \cdots, g_{m_{\mathrm{U}},M}e^{-\jmath\frac{2\pi f}{c}(d_{m_{\mathrm{U}},M} - d_{m_{\mathrm{U}}})}\right]^T$. Note that $|g_{m_{\mathrm{U}},m}| = \frac{c}{4\pi f d_{m_{\mathrm{U}},m}}$

denotes the free-space large-scale path loss between the m-th array of the BS and the m_{U}-th antenna of the U, $d_{m_{\mathrm{U}}}$ denotes the reference distance from $(0,0,0)$ to $(x_{\mathrm{U}}, y_{\mathrm{U}}+\tilde{m}_{\mathrm{U}}d, 0)$, and the distance between the m-th array of the BS and the m_{U}-th antenna of the U is given by

$$\begin{aligned} d_{m_{\mathrm{U}},m} &= \sqrt{x_{\mathrm{U}}^2 + [\tilde{m}d - (y_{\mathrm{U}} + \tilde{m}_{\mathrm{U}}d)]^2}, \\ &= \sqrt{d_{m_{\mathrm{U}}}^2 + (\tilde{m}d)^2 - 2\tilde{m}d d_{m_{\mathrm{U}}} \sin\theta_{m_{\mathrm{U}}}}, \end{aligned} \tag{8}$$

where $\theta_{m_{\mathrm{U}}}$ denotes the azimuth angle of the m_{U}-th antenna of the U with respect to $(0,0,0)$. In the same way, the near-field wiretapping channel $\mathbf{H}_{\mathrm{B,E}}(d,\theta)$ can be obtained. For simplicity, we neglect (d,θ) in $\mathbf{H}_{\mathrm{B,U}}(d,\theta)$ and $\mathbf{H}_{\mathrm{B,E}}(d,\theta)$ in the following.

Remark 1: The near-field spherical-wave channels derived in (7) and (8) contain the distance information of the U and the E, which facilitates distinguishing $\mathbf{H}_{\mathrm{B,U}}$ and $\mathbf{H}_{\mathrm{B,E}}$. Thus, the beam focusing can be utilized to achieve a positive gap of channel capacities between $\mathbf{H}_{\mathrm{B,U}}$ and $\mathbf{H}_{\mathrm{B,E}}$. This is entirely different from the far-field communications [8]–[10] that $\mathbf{H}_{\mathrm{B,U}}$ and $\mathbf{H}_{\mathrm{B,E}}$ are highly correlated in the angular domain.

C. Problem Formulation

In this letter, we aim to maximize the secrecy capacity subject to the analog phase-shift constraints and the transmit power budget of the baseband digital beamformers. The problem formulation is given by

$$\begin{aligned} \max_{\mathbf{P},\mathbf{W}} \quad & \log_2 \det\left(\mathbf{I}_{M_{\mathrm{U}}} + \sigma^{-2}\mathbf{H}_{\mathrm{B,U}}\mathbf{P}\mathbf{W}\mathbf{W}^H\mathbf{P}^H\mathbf{H}_{\mathrm{B,U}}^H\right) \\ & - \log_2 \det\left(\mathbf{I}_{M_{\mathrm{E}}} + \sigma^{-2}\mathbf{H}_{\mathrm{B,E}}\mathbf{P}\mathbf{W}\mathbf{W}^H\mathbf{P}^H\mathbf{H}_{\mathrm{B,E}}^H\right) && \text{(9a)} \\ \text{s.t.} \quad & \|\tilde{\mathbf{W}}\|_{\mathrm{F}}^2 \le P_{\max}, && \text{(9b)} \\ & p_{i,j} \in \mathcal{P}, 1 \le i \le M, \quad 1 \le j \le M_{\mathrm{R}}, && \text{(9c)} \end{aligned}$$

where $\tilde{\mathbf{W}} \triangleq \mathbf{P}\mathbf{W}$, and $P_{\max}$ denotes the maximal transmit power at the BS.

III. Secure Beam Focusing Design

In this section, we investigate the secure beam focusing of the considered near-field system. A two-stage algorithm is developed to optimize the hybrid beamformers. In particular, the block coordinate descent (BCD) approach is employed to design the fully-digital beamformers in the first stage. Then, the analog phase shifts and digital baseband precoders are alternately derived in closed-form expressions.

A. Stage-I: Fully-Digital Beamformer Design

To provide a performance upper bound for the proposed hybrid architecture, we concentrate on the fully-digital beamformer design in the first stage, where the analog phase-shift constraints are neglected and only the transmit power budget is considered. Accordingly, the problem (9) is reformulated as

$$\begin{aligned} \max_{\mathbf{W}_{\mathrm{FD}}} \quad & C_{\mathrm{s}} && \text{(10a)} \\ \text{s.t.} \quad & \mathrm{Tr}(\mathbf{W}_{\mathrm{FD}}\mathbf{W}_{\mathrm{FD}}^H) \le P_{\max}. && \text{(10b)} \end{aligned}$$

For notational convenience, we enable $\tilde{\mathbf{H}}_{\mathrm{B,U}} = \sigma^{-1}\mathbf{H}_{\mathrm{B,U}}$ and $\tilde{\mathbf{H}}_{\mathrm{B,E}} = \sigma^{-1}\mathbf{H}_{\mathrm{B,E}}$. Thus, the objective function (10a) can be expressed as $C_{\mathrm{s}} = \log_2\det(\mathbf{I}_{M_{\mathrm{U}}} + \tilde{\mathbf{H}}_{\mathrm{B,U}}\mathbf{W}_{\mathrm{FD}}\mathbf{W}_{\mathrm{FD}}^H\tilde{\mathbf{H}}_{\mathrm{B,U}}^H) - \log_2\det(\mathbf{I}_{M_{\mathrm{E}}} + \tilde{\mathbf{H}}_{\mathrm{B,E}}\mathbf{W}_{\mathrm{FD}}\mathbf{W}_{\mathrm{FD}}^H\tilde{\mathbf{H}}_{\mathrm{B,E}}^H)$. Note that the problem (10) is challenging to solve due to the intractable Shannon capacity expression in objective function (10a) and the quadratical power constraint (10b). To efficiently tackle this problem, the BCD method is adopted to iteratively solve the problem.

Lemma 1: Define a matrix function $\mathbb{F}(\mathbf{U},\mathbf{W}) \triangleq (\mathbf{I} - \mathbf{U}^H\mathbf{H}\mathbf{W})(\mathbf{I} - \mathbf{U}^H\mathbf{H}\mathbf{W})^H + \mathbf{U}^H\mathbf{U}$, the following equalities hold.

1) The positive definite matrix $\mathbf{V} = (\mathbb{F}(\mathbf{U},\mathbf{W}))^{-1}$ satisfies

$$\begin{aligned} \log\det(\mathbf{I} + \mathbf{H}\mathbf{W}\mathbf{W}^H\mathbf{H}^H) = \max_{\mathbf{V}\succ\mathbf{0},\mathbf{U}} \log\det(\mathbf{V}) - \\ \mathrm{Tr}(\mathbf{V}\mathbb{F}(\mathbf{U},\mathbf{W})) + m, \end{aligned} \tag{11}$$

where $\mathbf{U} = (\mathbf{I} + \mathbf{H}\mathbf{W}\mathbf{W}^H\mathbf{H}^H)^{-1}\mathbf{H}\mathbf{W}$.

2) For any positive definite matrix $\mathbf{E} \in \mathbb{C}^{m\times m}$, we have

$$-\log\det(\mathbf{E}) = \max_{\mathbf{V}\succ\mathbf{0}} \log\det(\mathbf{V}) - \mathrm{Tr}(\mathbf{V}\mathbf{E}) + m, \tag{12}$$

where $\mathbf{V} = \mathbf{E}^{-1}$.

Proof: Please see the proof in [10, Lemma 4.1]. ∎

By substituting $\mathbf{H} = \tilde{\mathbf{H}}_{\mathrm{B,E}}$, $\mathbf{W} = \mathbf{W}_{\mathrm{FD}}$ into (11) and $\mathbf{E} = \mathbf{I}_{M_{\mathrm{E}}} + \tilde{\mathbf{H}}_{\mathrm{B,E}}\mathbf{W}_{\mathrm{FD}}\mathbf{W}_{\mathrm{FD}}^H\tilde{\mathbf{H}}_{\mathrm{B,E}}^H$ into (12), the problem (10) can be reformulated as

$$\begin{aligned} \max_{\mathbf{W}_{\mathrm{FD}},\mathbf{V}_{\mathrm{U}}\succ\mathbf{0},\mathbf{V}_{\mathrm{E}}\succ\mathbf{0},\mathbf{U}} \quad & \log\det(\mathbf{V}_{\mathrm{U}}) - \mathrm{Tr}(\mathbf{V}_{\mathrm{U}}\mathbb{F}_{\mathrm{U}}(\mathbf{U},\mathbf{W}_{\mathrm{FD}})) + K \\ + \log\det(\mathbf{V}_{\mathrm{E}}) - \mathrm{Tr}(\mathbf{V}_{\mathrm{E}}(\mathbf{I}_{M_{\mathrm{E}}} + \tilde{\mathbf{H}}_{\mathrm{B,E}}\mathbf{W}_{\mathrm{FD}}\mathbf{W}_{\mathrm{FD}}^H\tilde{\mathbf{H}}_{\mathrm{B,E}}^H)) + M_{\mathrm{E}} && \text{(13a)} \\ \text{s.t.} \quad \mathrm{Tr}(\mathbf{W}_{\mathrm{FD}}\mathbf{W}_{\mathrm{FD}}^H) \le P_{\max}, && \text{(13b)} \end{aligned}$$

where $\{\mathbf{U},\mathbf{V}_{\mathrm{U}},\mathbf{V}_{\mathrm{E}}\}$ are the introduced auxiliary variables, and $\mathbb{F}_{\mathrm{U}}(\mathbf{U},\mathbf{W}_{\mathrm{FD}}) \triangleq (\mathbf{I} - \mathbf{U}^H\tilde{\mathbf{H}}_{\mathrm{B,U}}\mathbf{W}_{\mathrm{FD}})(\mathbf{I} - \mathbf{U}^H\tilde{\mathbf{H}}_{\mathrm{B,U}}\mathbf{W}_{\mathrm{FD}})^H + \mathbf{U}^H\mathbf{U}$. In the following, we solve the problem (13) iteratively by employing the BCD approach. To elaborate, the optimization variables are divided into three blocks, i.e., $\{\mathbf{U}\}$, $\{\mathbf{V}_{\mathrm{U}},\mathbf{V}_{\mathrm{E}}\}$ and $\{\mathbf{W}_{\mathrm{FD}}\}$. In each iteration, we optimize the optimization variables in one block while remaining the other blocks constant.

1) Subproblem with respect to $\{\mathbf{U}\}$*:* By fixing $\{\mathbf{V}_{\mathrm{U}},\mathbf{V}_{\mathrm{E}}\}$ and $\{\mathbf{W}_{\mathrm{FD}}\}$, the problem (13) is reduced to $\min_{\mathbf{U}} \ \mathrm{Tr}(\mathbf{V}_{\mathrm{U}}\mathbb{F}_{\mathrm{U}}(\mathbf{U},\mathbf{W}_{\mathrm{FD}}))$. According to Lemma 1, the optimal solution of $\mathbf{U}$ can be derived in the following expression.

$$\mathbf{U}^* = (\mathbf{I}_{M_{\mathrm{U}}} + \tilde{\mathbf{H}}_{\mathrm{B,U}}\mathbf{W}_{\mathrm{FD}}\mathbf{W}_{\mathrm{FD}}^H\tilde{\mathbf{H}}_{\mathrm{B,U}}^H)^{-1}\tilde{\mathbf{H}}_{\mathrm{B,U}}\mathbf{W}_{\mathrm{FD}}. \tag{14}$$

2) Subproblem with respect to $\{\mathbf{V}_U,\mathbf{V}_E\}$*:* With fixed $\{\mathbf{U}\}$ and $\{\mathbf{W}_{\mathrm{FD}}\}$, the problem (13) is reduced to two separate subproblems, i.e., $\max_{\mathbf{V}_{\mathrm{U}}} \ \log\det(\mathbf{V}_{\mathrm{U}}) - \mathrm{Tr}(\mathbf{V}_{\mathrm{U}} \succeq \mathbf{0}\mathbb{F}_{\mathrm{U}}(\mathbf{U},\mathbf{W}_{\mathrm{FD}}))$ and $\max_{\mathbf{V}_{\mathrm{E}}\succeq\mathbf{0}} \ \log\det(\mathbf{V}_{\mathrm{E}}) - \mathrm{Tr}(\mathbf{V}_{\mathrm{E}}(\mathbf{I}_{M_{\mathrm{E}}} + \tilde{\mathbf{H}}_{\mathrm{B,E}}\mathbf{W}_{\mathrm{FD}}\mathbf{W}_{\mathrm{FD}}^H\tilde{\mathbf{H}}_{\mathrm{B,E}}^H))$. With condition for the equal sign to hold, we can derive the optimal solution of $\{\mathbf{V}_{\mathrm{U}},\mathbf{V}_{\mathrm{E}}\}$, which is given by

$$\mathbf{V}_{\mathrm{U}}^* = \left((\mathbf{I} - \mathbf{U}^H\tilde{\mathbf{H}}_{\mathrm{B,U}}\mathbf{W}_{\mathrm{FD}})(\mathbf{I} - \mathbf{U}^H\tilde{\mathbf{H}}_{\mathrm{B,U}}\mathbf{W}_{\mathrm{FD}})^H + \mathbf{U}^H\mathbf{U}\right)^{-1}, \tag{15}$$

$$\mathbf{V}_{\mathrm{E}}^* = \left(\mathbf{I}_{M_{\mathrm{E}}} + \tilde{\mathbf{H}}_{\mathrm{B,E}}\mathbf{W}_{\mathrm{FD}}\mathbf{W}_{\mathrm{FD}}^H\tilde{\mathbf{H}}_{\mathrm{B,E}}^H\right)^{-1}. \tag{16}$$

3) Subproblem with respect to $\{\mathbf{W}_{FD}\}$: Solving problem (13) for $\mathbf{W}_{\text{FD}}$ with given $\{\mathbf{U}\}$ and $\{\mathbf{V}_{\text{U}}, \mathbf{V}_{\text{E}}\}$ is equivalent to the following subproblem.

$$\begin{aligned}\min_{\mathbf{W}_{\text{FD}}} \quad & \text{Tr}(\mathbf{V}_{\text{U}}\mathbb{F}_{\text{U}}(\mathbf{U}, \mathbf{W}_{\text{FD}}))+ \\ & \text{Tr}(\mathbf{V}_{\text{E}}(\mathbf{I}_{M_{\text{E}}} + \tilde{\mathbf{H}}_{\text{B,E}}\mathbf{W}_{\text{FD}}\mathbf{W}_{\text{FD}}^H\tilde{\mathbf{H}}_{\text{B,E}}^H)) \quad (17a) \\ \text{s.t.} \quad & \text{Tr}(\mathbf{W}_{\text{FD}}\mathbf{W}_{\text{FD}}^H) \le P_{\max}, \quad (17b)\end{aligned}$$

Note problem (17) is a convex a second-order cone programming (SOCP) program, which can be optimally solved. However, the near-field systems are usually accompanied by extremely large-scale antenna arrays. It indicates that directly solving the problem (17) possesses a high computational complexity, which is not applicable in practice. Since problem (17) is convex and satisfies Slater's condition, the strong duality holds between the original problem and the dual problem. Thus, we can obtain the optimal solution of problem (17) by solving its dual problem, where the Lagrangian function with respect to $\mathbf{W}_{\text{FD}}$ is given by

$$\begin{aligned}\mathcal{L}(\mathbf{W}_{\text{FD}}, \mu) = & \text{Tr}(\mathbf{W}_{\text{FD}}\tilde{\mathbf{H}}_{\text{B,U}}^H\mathbf{U}\mathbf{V}_{\text{U}}\mathbf{U}^H\tilde{\mathbf{H}}_{\text{B,U}}\mathbf{W}_{\text{FD}}^H)- \\ & \text{Tr}(\mathbf{V}_{\text{U}}\mathbf{U}^H\tilde{\mathbf{H}}_{\text{B,U}}\mathbf{W}_{\text{FD}}) - \text{Tr}(\mathbf{V}_{\text{U}}\mathbf{W}_{\text{FD}}^H\tilde{\mathbf{H}}_{\text{B,U}}^H\mathbf{U})+ \\ & \text{Tr}(\mathbf{W}_{\text{FD}}\tilde{\mathbf{H}}_{\text{B,E}}^H\mathbf{V}_{\text{E}}\tilde{\mathbf{H}}_{\text{B,E}}\mathbf{W}_{\text{FD}}^H) + \mu(\text{Tr}(\mathbf{W}_{\text{FD}}\mathbf{W}_{\text{FD}}^H) - P_{\max}), \quad (18)\end{aligned}$$

where $\mu \ge 0$ is the Lagrangian multiplier. By defining $f(\mu) = \min_{\mathbf{W}_{\text{FD}}} \mathcal{L}(\mathbf{W}_{\text{FD}}, \mu)$, the dual problem is given by

$$\begin{aligned}\max_{\mu} \quad & f(\mu) \quad (19a) \\ \text{s.t.} \quad & \mu \ge 0. \quad (19b)\end{aligned}$$

Note that the optimal solution of $\mathbf{W}_{\text{FD}}$ under any given $\mu > 0$ can be derived by adopting the first-order optimality condition, i.e.,

$$\mathbf{W}_{\text{FD}}^*(\mu) = \mathbf{E}(\mu\mathbf{I}_M + \mathbf{D})^{-1}\mathbf{E}^H\tilde{\mathbf{H}}_{\text{B,U}}^H\mathbf{U}\tilde{\mathbf{H}}_{\text{B,U}}. \quad (20)$$

Then, by carrying out the one-dimensional search for μ, the fully-digital beamformer $\mathbf{W}_{\text{FD}}$ can be obtained.

Remark 2: In general, the one-dimensional search for (20) suffers high computational complexity as the inverse matrix operation $(\mu\mathbf{I}_M + \mathbf{D})^{-1}$ incurs the complexity of $\mathcal{O}(M^3)$. However, since $\mathbf{EDE}^H$ is the result of the eigenvalue decomposition of $\tilde{\mathbf{H}}_{\text{B,U}}^H\mathbf{U}\mathbf{V}_{\text{U}}\mathbf{U}^H\tilde{\mathbf{H}}_{\text{B,U}} + \tilde{\mathbf{H}}_{\text{B,E}}^H\mathbf{V}_{\text{U}}\tilde{\mathbf{H}}_{\text{B,E}}$, it can readily observe that both $\mathbf{D}$ and $\mu\mathbf{I}_M$ are diagonal matrices, and inverse matrix $(\mu\mathbf{I}_M+\mathbf{D})^{-1}$ can be rewritten as a diagonal matrix $\bar{\mathbf{D}}_\mu$, where the i-th diagonal element of $\bar{\mathbf{D}}_\mu$ is given by $\bar{\mathbf{D}}_\mu^{[i,i]} = \frac{1}{\mu+\mathbf{D}^{i,i}}$. Thus, we can directly calculate $\bar{\mathbf{D}}_\mu$ to update $\mathbf{W}_{\text{FD}}^*(\mu)$ in the one-dimensional search, which is computationally efficient.

B. Stage-II: Hybrid Beamformer Design

In this subsection, we focus on the design of the hybrid beamformers. To approximately maximize the secrecy mutual information between the BS and U, we project the optimized $\mathbf{W}_{\text{FD}}$ to the set of hybrid beamformers to obtain the near-optimal analog phase shifters and baseband precoders. The hybrid beamformer design problem is given by

$$\begin{aligned}\min_{\mathbf{P},\mathbf{W}} \quad & \|\mathbf{W}_{\text{FD}} - \mathbf{P}\mathbf{W}\|_{\text{F}}^2 \quad (21a) \\ \text{s.t.} \quad & p_{i,j} \in \mathcal{P}, 1 \le i \le M, \quad 1 \le j \le M_{\text{R}}. \quad (21b)\end{aligned}$$

Algorithm 1 Two-stage algorithm.

1: Initialize initial $\mathbf{P}$ and $\mathbf{W}_{\text{FD}}$ with $n = 1$ and $m = 1$. Set the convergence accuracy ϵ_1, ϵ_2, and ϵ_3.
2: **BCD repeat**
3: update $\mathbf{U}^n$ according to (14).
4: update $\{\mathbf{V}_{\text{U}}^n, \mathbf{V}_{\text{E}}^n\}$ according to (15) and (16).
5: update $\mathbf{W}_{\text{FD}}^n$ by carrying out the Bisection search with the accuracy of ϵ_3.
6: set $n = n + 1$.
7: **until** the $|C_{\text{s}}(\mathbf{W}_{\text{FD}}^n) - C_{\text{s}}(\mathbf{W}_{\text{FD}}^{n-1})| \le \epsilon_1$.
8: **AO repeat**
9: update $\mathbf{W}^m$ according to (22).
10: iteratively update $p(i,j)^m$ according to (25).
11: set $m = m + 1$.
12: **until** the $|C_{\text{s}}(\mathbf{P}^m\mathbf{W}^m) - C_{\text{s}}(\mathbf{P}^{m+1}\mathbf{W}^{m+1})| \le \epsilon_2$.

Note that with any feasible fully-digital beamformer $\mathbf{W}_{\text{FD}} \le P_{\max}$, the hybrid beamformer optimized based on problem (21) must satisfy the requirement of being sufficiently "close" to $\mathbf{W}_{\text{FD}}$ [14]. Thus, no additional power constraint is required for the problem (21). Since problem (21) is a highly coupled quadratic problem, we consider adopting the alternating optimization (AO) framework to iteratively optimize the digital baseband precoder and the analog phase shifters.

1) Digital Baseband Precoder Design: With the fixed $\mathbf{P}$, the problem (21) is reduced to $\min_{\mathbf{W}} \|\mathbf{W}_{\text{FD}} - \mathbf{P}\mathbf{W}\|_{\text{F}}^2$, which can be optimally solved by adopting the first-order optimality condition. As such, the optimal $\mathbf{W}$ is given by

$$\mathbf{W}^* = (\mathbf{P}^H\mathbf{P})^{-1}\mathbf{P}^H\mathbf{W}_{\text{FD}}. \quad (22)$$

2) Analog Phase Shifter Design: With the fixed $\mathbf{W}$, the problem (21) can be reduced as

$$\begin{aligned}\min_{\mathbf{P}} \quad & \text{Tr}(\mathbf{P}^H\mathbf{P}\mathbf{X}) - 2\Re(\text{Tr}(\mathbf{P}\mathbf{Y})) \quad (23a) \\ \text{s.t.} \quad & p_{i,j} \in \mathcal{P}, 1 \le i \le M, \quad 1 \le j \le M_{\text{R}}, \quad (23b)\end{aligned}$$

where $\mathbf{X} = \mathbf{W}\mathbf{W}^H$ and $\mathbf{Y} = \mathbf{W}_{\text{FD}}\mathbf{W}^H$. Since the variable $p_{i,j}$ are separable in the unit-modulus constraint (23b), the problem (23) can be efficiently tackled by the BCD method, which iteratively optimizes each entry of $\mathbf{P}$ while fixing the remaining elements. Consequently, the subproblem with respect to $p_{i,j}$ is given by

$$\max_{|p_{i,j}|=1} \quad \Re(\bar{z}_{i,j}p_{i,j}), \quad (24a)$$

where $z_{i,j}$ is a complex coefficient determined by the elements of $\mathbf{P}$ except for $p_{i,j}$. Under the unit-modulus constraint, the optimal $p_{i,j}$ can be derived as follows.

$$p_{i,j}^* = \frac{z_{i,j}}{|z_{i,j}|}, \quad (25)$$

where $z_{i,j} = \mathbf{Y}_{[i,j]} - (\tilde{\mathbf{X}}_{[i,j]} - p_{i,j}\mathbf{X}_{[j,j]})$ and $\tilde{\mathbf{X}} = \mathbf{P}\mathbf{X}$. Afterward, by alternatingly updating $\mathbf{W}$ and $p_{i,j}$, the digital baseband precoders and analog phase shifters can be determined.

C. Overall Algorithm

The proposed two-stage algorithm is summarized in **Algorithm 1**. For the BCD loop in **Algorithm 1**, since the optimal solutions $\{\mathbf{U}\}$ and $\{\mathbf{V}_{\mathrm{U}}, \mathbf{V}_{\mathrm{E}}\}$ and the Karush-Kuhn-Tucker (KKT) point solution $\{\mathbf{W}_{\mathrm{FD}}\}$ are guaranteed in steps 3, 4 and 5, we readily have the following inequality

$$\begin{aligned} C_{\mathrm{s}}(\mathbf{U}^n, \mathbf{V}_{\mathrm{U}}^n, \mathbf{V}_{\mathrm{E}}^n, \mathbf{W}_{\mathrm{FD}}^n) \geq C_{\mathrm{s}}(\mathbf{U}^{n+1}, \mathbf{V}_{\mathrm{U}}^n, \mathbf{V}_{\mathrm{E}}^n, \mathbf{W}_{\mathrm{FD}}^n) \geq \\ C_{\mathrm{s}}(\mathbf{U}^{n+1}, \mathbf{V}_{\mathrm{U}}^{n+1}, \mathbf{V}_{\mathrm{E}}^{n+1}, \mathbf{W}_{\mathrm{FD}}^n) \geq \\ C_{\mathrm{s}}(\mathbf{U}^{n+1}, \mathbf{V}_{\mathrm{U}}^{n+1}, \mathbf{V}_{\mathrm{E}}^{n+1}, \mathbf{W}_{\mathrm{FD}}^{n+1}), \end{aligned} \tag{26}$$

which proves the monotonic convergence of the generated sequence $\{C_{\mathrm{s}}^n, \cdots, C_{\mathrm{s}}^{n+m}, \cdots\}$ with $C_{\mathrm{s}}^n = C_{\mathrm{s}}(\mathbf{U}^n, \mathbf{V}_{\mathrm{U}}^n, \mathbf{V}_{\mathrm{E}}^n, \mathbf{W}_{\mathrm{FD}}^n)$. Furthermore, by checking the KKT conditions, it is readily known that the accumulation point $\bar{C}_{\mathrm{s}}$ of the sequence $\{C_{\mathrm{s}}^n, \cdots, C_{\mathrm{s}}^{n+m}, \cdots\}$ is the KKT solution of the original problem [10, Proposition 4.2]. In the same way, we can prove that the AO alternating iteration converges to at least the stationary point solution of the problem (21).

Since all the subproblems are solved by the closed-form solutions, the proposed two-stage algorithm is complexity-efficient. The main complexity of the proposed two-stage algorithm relies on the eigenvalue decomposition operation and inverse matrix operation, the whole complexity is given by $\mathcal{O}\Big(l_1(K^3 + M_{\mathrm{R}}^3 + (l_{\mathrm{B}}+1)M^3) + l_2 K^3\Big)$ [15], where l_1, l_{B} and l_2 denote the number of iterations of the BCD loop, the Bisection algorithm, and the AO loop.

Furthermore, it is easy to modify the proposed algorithm to the network with multiple users and eavesdroppers, where each legitimate user will be interfered with by signals of other legitimate users. For the non-colluding eavesdropping case, the weighted minimum mean-square error (WMMSE) approach [16] and the equality (12) in Lemma 1 can be employed to deal with the non-convex achievable rate expressions at the legitimate users and eavesdroppers. For the colluding eavesdropping case, the multiple eavesdroppers can be equivalently regarded as a virtual eavesdropping node, which is equipped with as many antennas as the sum of the antennas of all the eavesdroppers. Thus, the achievable rate expressions at eavesdroppers have the same mathematical form as the single-eavesdropper case, which can be directly tackled by the proposed algorithm.

IV. Numerical Results

This section provides the numerical results to validate the effectiveness of the proposed scheme. The linear topology is considered for the simulations, where the midpoint of the BS antenna is located in (0,0,0) meter (m), while midpoints of the antennas of U and E are respectively located 15 m and 5 m from the coordinate (0,0,0) m with the azimuth angle of 45°. All the ULAs are positioned along the y-axis. Unless otherwise specified, the default parameters are set as $f = 28$ GHz, $d = \frac{\lambda}{2}$, $M = 256$, $M_{\mathrm{U}} = 8$, $M_{\mathrm{E}} = 8$, $M_{\mathrm{R}} = 8$, $K = 4$, $\sigma^2 = -105$ dBm, $\epsilon_1 = 10^{-4}$ and $\epsilon_2 = \epsilon_3 = 10^{-6}$. The numerical results are averaged from 100 independent Monte-Carlo experiments.

Fig. 3 illustrates the secrecy performance of the proposed algorithm, where two baseline schemes are considered for performance comparison. The first scheme is the maximum-ratio transmission (MRT), where the singular value decomposition (SVD) and water-filling algorithm are employed to maximize the achievable rate at the U. The second scheme is the analog-aligning-based hybrid beamforming (AAHB) scheme, where the analog beamformer is aligned to the channel of the U and the baseband digital beamformer is optimized by our proposed BCD algorithm. From Fig. 3(b), we can observe that: 1) Even if the E is located between the BS and the U, the secure transmission can be guaranteed for all the schemes. It demonstrates that the near-field spherical-wave channel model brings new distance-domain security gains. 2) Increasing the antennas of the E degrades the secrecy performance of the network. This is because the rise of the number of antennas of E enhances the reception ability of E, which narrows the gap between the channel capacities of U and E.

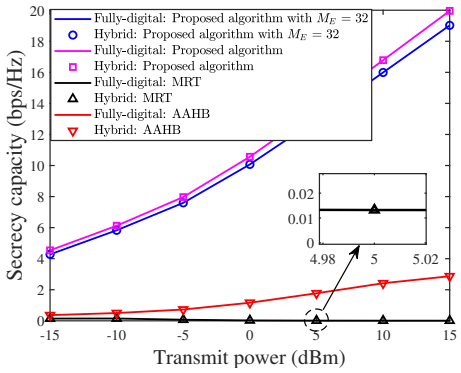

Fig. 3. Secrecy performance comparison versus $P_{\max}$ for different baseline schemes.

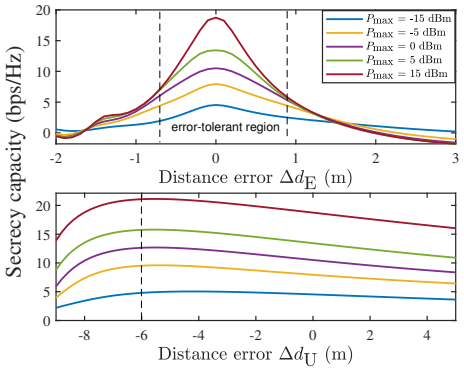

Fig. 4. Impact of the imperfect distance knowledge of E and U on the secrecy performance of the considered near-field network

Fig. 4 evaluates the impact of the imperfect distance knowledge of E and U on the secrecy performance, where the U and E are estimated to be located 15 m and 5 m from the BS. Here, the distance error is defined as the difference between the estimated distance and the practical distance, i.e., $\Delta d_\varsigma = d_\varsigma^{\mathrm{est}} - d_\varsigma^{\mathrm{pra}}$, $\varsigma \in \{\mathrm{E}, \mathrm{U}\}$. As shown in top side of Fig. 4, the secrecy capacity decreases with the increased $|\Delta d_{\mathrm{E}}|$. This is because when $|\Delta d_{\mathrm{E}}|$ increases, the optimized secrecy beamfocusing beamformers cannot accurately achieve the suppression of the signal at the location of the E, thus deteriorating the secrecy performance of the network. It can also be observed that when $|\Delta d_{\mathrm{E}}|$ exceeds the error-tolerant

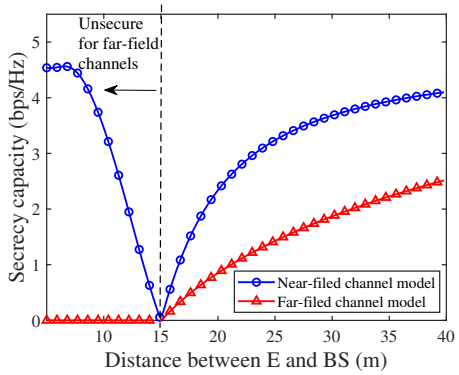

Fig. 5. Secrecy performance versus the location of E, where $P_{\max} = -15$ dBm.

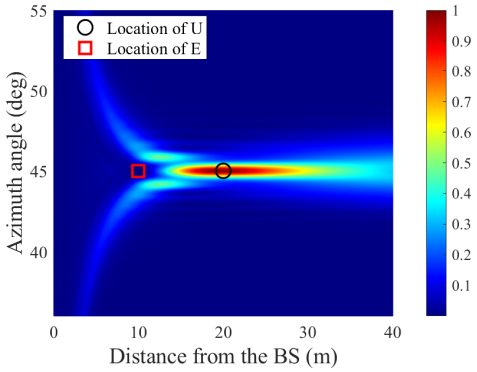

Fig. 6. Normalized signal power spectrum, where $P_{\max} = -15$ dBm, U is located 20 m from the BS, and E is located 10 m from the BS.

region, increasing the power will leak more signal to E, which degrades the secrecy performance of the network. From the bottom side of Fig. 4, the secrecy capacity reaches the maximum value when Δd_{E} is around -6 m, which is a counter-intuitive but predictable result. Specifically, although the non-accurate beam focusing beamformers are designed due to the imperfect distance information of the U, the practical U enjoys a much less large-scale path loss when $\Delta d_{\mathrm{E}} \approx -6$ m, which predominately enhances the secrecy performance of the network.

In Fig. 5, we present the secrecy capacity versus the location of E by adopting the far-field planar-wave channel model and near-field spherical-wave channel model, respectively. It can be seen that when adopting far-field channels, the perfectly secure transmission will only occur if the eavesdropping links suffer worse channel conditions than the legitimate links, which however is always guaranteed when adopting near-field channels. This is because the near-field channels bring the new distance-domain security gains, which rely on the distance disparity of the E with respect to the reference point of the U. Also can be observed, that adopting near-field channels achieves a higher secrecy rate than far-field channels even when the eavesdropper is located farther away from the BS than the legitimate user. This is expected because the accurate spherical-wave channel contains the extra distance information, which facilitates focusing the signal energy on the legitimate user while suppressing the signal leakage to the eavesdropper.

To further illustrate the impact of beam focusing in near-field communications, Fig. 6 plots the normalized signal power spectrum over the free-space location. As can be observed, the optimized beamformers can directionally enhance the signal power at the direction of $45°$. Meanwhile, we can also see that at a distance of 10 m, i.e. at the position of E, the signal is fully suppressed, while at a distance of 20 m, the signal power is significantly strengthened. This result demonstrates that the proposed secure beam focusing scheme can precisely enhance the signal strength at a specific point of free space without significant energy/information leakage on the incident pathes.

V. Conclusion

A novel secure near-field framework was proposed. A two-stage algorithm was developed to maximize the secrecy capacity of the U via jointly optimizing unit-modulus phase shifters and baseband digital beamformers. Numerical results were presented to unveil that the secrecy performance of near-field communications is primarily relevant to the relative distance of the E with respect to the U.

References

[1] Y. Liu, Z. Wang, et al, "Near-field communications: A tutorial review," *IEEE Open J. Commun. Soc.*, vol. 4, pp. 1999–2049, 2023.

[2] H. Zhang, N. Shlezinger, et al, "Beam focusing for near-field multiuser MIMO communications," *IEEE Trans. Wireless Commun.*, vol. 21, no. 9, pp. 7476–7490, Sep. 2022.

[3] Z. Wu, M. Cui, Z. Zhang, and L. Dai, "Distance-aware precoding for near-field capacity improvement in XL-MIMO," in *Proc. IEEE 95th Veh. Technol. Conf. (VTC-Spring)*, Jun. 2022, pp. 1–5.

[4] Z. Wang, X. Mu, and Y. Liu, "Near-field integrated sensing and communications," *IEEE Commun. Lett.*, vol. 27, no. 8, pp. 2048–2052, Aug. 2023.

[5] X. Gan, C. Huang, Z. Yang, C. Zhong, and Z. Zhang, "Near-field localization for holographic RIS assisted mmWave systems," *IEEE Commun. Lett.*, vol. 27, no. 1, pp. 140–144, Jan. 2023.

[6] X. Mu, J. Xu, et al, "Reconfigurable intelligent surface-aided near-field communications for 6G: Opportunities and challenges," *IEEE Veh. Technol. Mag.*, early access, doi: 10.1109/MVT.2023.3345608.

[7] X. Pang, M. Liu, et al, "Secrecy analysis of UAV-based mmWave relaying networks," *IEEE Trans. Wireless Commun.*, vol. 20, no. 8, pp. 4990–5002, Aug. 2021.

[8] Y. Liu, Z. Qin, et al, "Enhancing the physical layer security of non-orthogonal multiple access in large-scale networks," *IEEE Trans. Wireless Commun.*, vol. 16, no. 3, pp. 1656–1672, Mar. 2017.

[9] Z. Zhang, J. Chen, Y. Liu, Q. Wu, B. He, and L. Yang, "On the secrecy design of STAR-RIS assisted uplink NOMA networks," *IEEE Trans. Wireless Commun.*, vol. 21, no. 12, pp. 11207–11221, Dec. 2022.

[10] Q. Shi, W. Xu, et al, "Secure beamforming for MIMO broadcasting with wireless information and power transfer," *IEEE Trans. Wireless Commun.*, vol. 14, no. 5, pp. 2841–2853, May. 2015.

[11] G. J. Anaya-Lpez, J. P. Gonzlez-Coma, et al, "Spatial degrees of freedom for physical layer security in XL-MIMO," in *Proc. IEEE 95th Veh. Technol. Conf. (VTC-Spring)*, Helsinki, Finland, Jun. 2022, pp. 1-5

[12] Z. Xie, Y. Liu, et al, "Performance analysis for near-field MIMO: Discrete and continuous aperture antennas," *IEEE Wireless Commun. Lett.*, vol. 12, no. 12, pp. 2258–2262, Dec. 2023.

[13] X. Wei and L. Dai, "Channel estimation for extremely large-scale massive MIMO: Far-field, near-field, or hybrid-field?" *IEEE Commun. Lett.*, vol. 26, no. 1, pp. 177–181, Jan. 2022.

[14] X. Yu, J. -C. Shen, et al, "Alternating minimization algorithms for hybrid precoding in millimeter wave MIMO systems," *IEEE J. Sel. Top. Signal Process.*, vol. 10, no. 3, pp. 485–500, Apr. 2016.

[15] J. Nocedal and S. Wright, *Numerical optimization*. New York, NY, USA: Springer-Verlag, 2006.

[16] Q. Shi and M. Hong, "Spectral efficiency optimization for millimeter wave multiuser MIMO systems," *IEEE J. Sel. Topics Signal Process.*, vol. 12, no. 3, pp. 455–468, Jun. 2018.